ELSEVIER

Advances in Engineering Software 33 (2002) 445–452

ADVANCES IN ENGINEERING SOFTWARE

www.elsevier.com/locate/advengsoft

Solving laminated plates by domain decomposition

J. Kruis[a,*], K. Matouš[b,1], Z. Dostál[c,2]

[a]*Department of Structural Mechanics, Faculty of Civil Engineering, Czech Technical University in Prague, Thákurova 7, 166 29 Prague, Czech Republic*
[b]*Department of Mechanical Aerospace and Nuclear Engineering, Rensselaer Polytechnic Institute, 5003 Jonsson Engineering Center, 110 8th Street, Troy, NY 12180, USA*
[c]*Department of Applied Mathematics, Faculty of Electrical Engineering, Technical University Ostrava, 17. listopadu, 708 33 Ostrava-Poruba, Czech Republic*

Received 16 November 2000; accepted 1 July 2002

Abstract

The refined Mindlin-Reissner theory is used to estimate the overall response of composite plates. The difficulties with the solution of a system of algebraic equations, which emerged in analysis of composite materials, are studied and a special version of decomposition is proposed. Similarity between the system of equations derived from the layered theory and from the finite element tearing and interconnecting method suggests a strategy for implementation in the parallel environment. Several applications are investigated and a number of numerical results are presented.

Keywords: Composite laminated plate; Multilayered plate element; Domain decomposition; Parallel computation

1. Introduction

The continuous development of composite materials, computer industry and the engineers' requirements for effective design in recent decades have led to searching for many different methods for improving design and the overall performance of composite structures. A large group of composite structures is represented by laminated plates, which are used in variety of applications and their effective analysis can provide substantial cost and labor reduction. Therefore, the present work is devoted to effective modeling of multilayered plates.

The two-dimensional laminated plate theories can be broadly classified into two main categories. The solution based on the Kirchhoff, Reissner or Mindlin hypotheses represent the first category. The second category consists of discrete layer theories based on piecewise approximation of field variables in the thickness direction. Continuity of transverse stresses at the ply interfaces is achieved either by imposing the displacement continuity conditions as a set of constraints [1], or by an explicit approximation of the transverse stresses within each layer. The methods of the first category lead to systems with smaller number of degrees of freedom compared to those from the second category, however, their accuracy is not as good especially for stress description.

The present work is devoted to the refined theory based on Mindlin's kinematic assumptions with the independent approximation of in-plane displacements within each layer. This theory was originally proposed by Mau [1] in 1972 and explored by Šejnoha [2]. The continuity of in-plane displacements at ply interfaces is attained by imposing interfacial constraints. These constraints are added into the modified variational principle through the Lagrange multipliers, which represent nodal forces. Derivation of a multilayered plate element is based on a special procedure for interpolating the transverse shear strains proposed by Hughes [3].

Application of numerical methods to engineering problems usually leads to large systems of equations. Despite the fast increase in processors performance, the requirements for advanced numerical computations are so high that they make parallel technologies a necessity. Symmetric multiprocessor PCs are becoming a standard commodity in the market. Their clusters represent currently the most perspective and progressive trend in the area of high-performance parallel systems. They are used as

* Corresponding author. Tel.: +420-2-2435-4369; fax: +420-2-2431-0775.
E-mail addresses: jk@cml.fsv.cvut.cz (J. Kruis), matouk@rpi.edu (K. Matouš), zdenek.dostal@vsb.cz (Z. Dostál).
[1] Tel.: +1-518-276-6204; fax: +1-518-276-8784.
[2] Tel.: +420-69-699-5227; fax: +420-69-691-9597.

0965-9978/02/$ - see front matter
PII: S0965-9978(02)00075-3

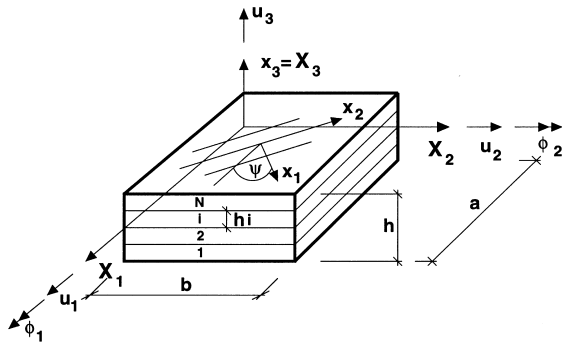

Fig. 1. Representative volume element.

network, database and computing servers. Thanks to these new technologies, many research teams have started to search for new algorithms, which are suitable to be applied in the parallel environment. Especially domain decomposition techniques appear to be very popular at this time. There are a lot of contributions to this research area in structural mechanics [4,5]. However, the domain decomposition methods in the analysis of composite materials and structures have not yet been fully utilized.

2. Basic theory of multilayered plates

Let us consider a fibrous composite plate composed of N orthotropic layers as in Fig. 1. The thickness of the plate and the ith layer are denoted as h and h^i, respectively. For the sake of simplicity we assume that identical boundary conditions are prescribed for all layers and that these conditions are sufficient to prevent the plate from rigid body motions. Such assumptions are exploited in the solution of the resulting system of linear equations only. However, using the standard finite element tearing and interconnecting (FETI) methodology, it is not difficult to apply our approach to the solution of more general problems.

To describe overall geometry of the plate, we introduce a Cartesian system with co-ordinates $\mathbf{X} = (X_1, X_2, X_3)$ located such that the X_3 co-ordinate is normal to the middle planes of the layers. In each layer, we define a local co-ordinate system $\mathbf{x}^i = (x_1^i, x_2^i, x_3^i)$, which complies with the axes of orthotropy defined by fibers. The following bold lower-case Greek letters $\boldsymbol{\varepsilon}$, $\boldsymbol{\sigma}$ denote the strain and stress vectors in the local co-ordinate system, whereas the bold upper-case letters $\mathbf{E}$, $\mathbf{S}$ represent the corresponding quantities in the overall co-ordinate system. The symbol $u^i_{1,j}$ is used to denote partial differentiation with respect to x_j.

2.1. Kinematic and constitutive equations

Let the displacement field of each layer satisfy the Mindlin kinematic assumptions with the independent approximation of in-plane displacements in the form

$$\begin{aligned} u_1^i(x_1,x_2,x_3) &= U_1^i(x_1,x_2) + x_3^i\phi_2^i(x_1,x_2),\ \ u_2^i(x_1,x_2,x_3) \\ &= U_2^i(x_1,x_2) - x_3^i\phi_1^i(x_1,x_2),\ \ u_3^i(x_1,x_2,x_3) \\ &= U_3^i(x_1,x_2), \\ i &= 1,2,\ldots,N, \end{aligned} \tag{1}$$

where the vector $\mathbf{U}^i = [U_1^i, U_2^i, U_3^i]^{\mathrm{T}}$ denotes the longitudinal and transverse displacements in the x_1^i, x_2^i and x_3^i directions and the ϕ_1^i, ϕ_2^i denote the rotations around the x_1^i and x_2^i axes, respectively.

To satisfy the continuity of in-plane displacements at the ply interfaces, we impose the following constraints

$$\begin{aligned} &U_1^i + \tfrac{1}{2}h^i\phi_2^i = U_1^{i+1} - \tfrac{1}{2}h^{i+1}\phi_2^{i+1},\ \ U_2^i - \tfrac{1}{2}h^i\phi_1^i \\ &\quad = U_2^{i+1} + \tfrac{1}{2}h^{i+1}\phi_1^{i+1},\ \ U_3^i = U_3^{i+1}, \\ &i = 1,2,\ldots,N-1. \end{aligned} \tag{2}$$

Thus the in-plane strain vector $\boldsymbol{\varepsilon}_{\mathrm{m}}^i = [\varepsilon_{11}^i, \varepsilon_{22}^i, \gamma_{12}^i]^{\mathrm{T}}$ can be written in the form

$$\boldsymbol{\varepsilon}_{\mathrm{m}}^i = \boldsymbol{\varepsilon}_{0\mathrm{m}}^i + x_3^i\boldsymbol{T}\boldsymbol{\kappa}^i, \tag{3}$$

$$\boldsymbol{\varepsilon}_{0\mathrm{m}}^i = [U_{1,1}^i, U_{2,2}^i, U_{1,2}^i + U_{2,1}^i]^{\mathrm{T}},$$

$$\boldsymbol{\kappa}^i = [\phi_{1,2}^i, \phi_{2,1}^i, \phi_{1,1}^i - \phi_{2,2}^i]^{\mathrm{T}},$$

where the orthogonal matrix $\boldsymbol{T}$ reads

$$\boldsymbol{T} = \begin{bmatrix} 0 & 1 & 0 \\ -1 & 0 & 0 \\ 0 & 0 & -1 \end{bmatrix}. \tag{4}$$

The out-of-plane strain vector $\boldsymbol{\varepsilon}_{\mathrm{s}}^i = [\varepsilon_{13}^i, \varepsilon_{23}^i]^{\mathrm{T}}$ is related to the displacement field by

$$\boldsymbol{\varepsilon}_{\mathrm{s}}^i = [U_{3,2}^i - \phi_1^i, U_{3,1}^i + \phi_2^i]^{\mathrm{T}} \tag{5}$$

and the ply constitutive relations in the local co-ordinates yield

$$\boldsymbol{\sigma}_{\mathrm{m}}^i = \mathbf{L}_{\mathrm{m}}^i(\boldsymbol{\varepsilon}_{\mathrm{m}}^i - \boldsymbol{\mu}_{\mathrm{m}}^i), \qquad \boldsymbol{\sigma}_{\mathrm{s}}^i = \mathbf{L}_{\mathrm{s}}^i(\boldsymbol{\varepsilon}_{\mathrm{s}}^i - \boldsymbol{\mu}_{\mathrm{s}}^i), \tag{6}$$

where $\mathbf{L}_{\mathrm{m}}^i$ denotes the (3×3) in-plane constitutive matrix, $\mathbf{L}_{\mathrm{s}}^i$ denotes the (2×2) out-of-plane constitutive matrix of the ply, and the vectors $\boldsymbol{\mu}_{\mathrm{m}}^i$ and $\boldsymbol{\mu}_{\mathrm{s}}^i$ denote eigenstrains in the plies caused by the inelastic effects, initial fiber pre-stressing and/or thermal effect. For the sake of simplicity, we assume that the eigenstrains are equal to zero. In the global co-ordinate system the stress vectors are denoted by

$$\mathbf{S}_{\mathrm{m}}^i = [\mathbf{S}_{11}^i, \mathbf{S}_{22}^i, \mathbf{S}_{12}^i]^{\mathrm{T}}, \qquad \mathbf{S}_{\mathrm{s}}^i = [\mathbf{S}_{13}^i, \mathbf{S}_{23}^i]^{\mathrm{T}}. \tag{7}$$

Similarly, after transformation of strain vectors $\boldsymbol{\varepsilon}_{0\mathrm{m}}^i$, $\boldsymbol{\kappa}^i$, $\boldsymbol{\varepsilon}_{\mathrm{s}}^i$, we obtain $\mathbf{E}_{0\mathrm{m}}^i$, $\bar{\boldsymbol{\kappa}}^i$, $\mathbf{E}_{\mathrm{s}}^i$.

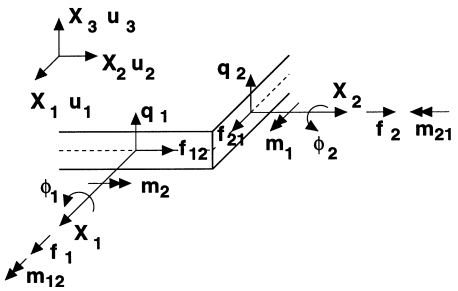

Fig. 2. Internal forces in the ply.

2.2. Internal forces

Once the stress vectors (7) are known, we can evaluate the internal forces within each lamina using the notation introduced in Fig. 2 where

$$\mathbf{f}^i = \int_{-h^i/2}^{h^i/2} \mathbf{S}^i_{\mathrm{m}}\, \mathrm{d}x_3 = \mathbf{A}^i \mathbf{E}^i_{0\mathrm{m}}, \tag{8}$$

$$\mathbf{m}^i = \boldsymbol{T}^{\mathrm{T}} \int_{-h^i/2}^{h^i/2} x_3^i \mathbf{S}^i_{\mathrm{m}}\, \mathrm{d}x_3 = \boldsymbol{T}^{\mathrm{T}} \mathbf{D}^i \boldsymbol{T} \bar{\boldsymbol{\kappa}}^i,$$

$$\mathbf{q}^i = \int_{-h^i/2}^{h^i/2} \mathbf{S}^i_{\mathrm{s}}\, \mathrm{d}x_3 = \mathbf{C}^i \mathbf{E}^i_{\mathrm{s}}$$

and $\mathbf{A}^i$, $\mathbf{D}^i$ and $\mathbf{C}^i$ are the transformed material stiffness matrices of the orders (3×3), (3×3) and (2×2), respectively.

2.3. Element matrices

The multilayered plate element will be derived by means of the total potential energy function

$$\Pi = U_{\mathrm{int}} + U_{\mathrm{ext}}, \tag{9}$$

where U_{ext} represents the work of external load and the term U_{int} after neglecting eigenstrains reads

$$U_{\mathrm{int}} = \frac{1}{2} \sum_{i=1}^{N} \int_{S_{\mathrm{m}}} [(\mathbf{E}^i_{0\mathrm{m}})^{\mathrm{T}} \mathbf{A} (\mathbf{E}^i_{0\mathrm{m}}) + (\boldsymbol{T}\bar{\boldsymbol{\kappa}}^i)^{\mathrm{T}} \mathbf{D}^i (\boldsymbol{T}\bar{\boldsymbol{\kappa}}^i) + (\mathbf{E}^i_{\mathrm{s}})^{\mathrm{T}} \mathbf{C}^i \mathbf{E}^i_{\mathrm{s}}] \mathrm{d}S_{\mathrm{m}}. \tag{10}$$

The finite element stiffness matrix may be obtained by varying the internal energy U_{int} (Eq. (10)). The finite element approximations of displacements are

$$u^i_1 = \sum_{a=1}^{n} N_a (U^i_1 + x^i_3 \phi^i_2)_a, \tag{11}$$

$$u^i_2 = \sum_{a=1}^{n} N_a (U^i_2 - x^i_3 \phi^i_1)_a,$$

$$u^i_3 = \sum_{a=1}^{n} N_a (U^i_3)_a,$$

where n denotes the number of nodes of one element and N_a represents a shape function. The strain vectors are interpolated in terms of nodal displacements $\mathbf{d}^i$ so that

$$\mathbf{E}^i_{0\mathrm{m}} = \mathbf{B}^u \mathbf{d}^i_u, \tag{12}$$

$$\bar{\boldsymbol{\kappa}}^i = \mathbf{B}^\phi \mathbf{d}^i_\phi,$$

$$\mathbf{E}^i_{\mathrm{s}} = \mathbf{B}^{s1} \mathbf{d}^i_\phi + \mathbf{B}^{s2} \mathbf{d}^i_w,$$

where

$$(\mathbf{d}^i_u)^{\mathrm{T}} = ({}^1U_1, {}^1U_2, \ldots, {}^nU_1, {}^nU_2)^i, \tag{13}$$

$$(\mathbf{d}^i_\phi)^{\mathrm{T}} = ({}^1\phi_1, {}^1\phi_2, \ldots, {}^n\phi_1, {}^n\phi_2)^i,$$

$$(\mathbf{d}^i_w)^{\mathrm{T}} = ({}^1U_3, \ldots, {}^nU_3)^i.$$

The geometric matrices $\mathbf{B}^u$, $\mathbf{B}^\phi$ are obtained from the standard finite element approximation and the matrices $\mathbf{B}^{s1}$, $\mathbf{B}^{s2}$ are based on the procedure for interpolating the transverse shear strains [3]. The detailed description of the plate element is given in Ref. [6].

Thus element stiffness matrix $\mathbf{K}^i$ of ith ply derived from Eq. (10) is a (20×20) square matrix of the form

$$\mathbf{K}^i = \begin{bmatrix} \mathbf{k}^i_u & 0 & 0 \\ 0 & \mathbf{k}^i_b + \mathbf{k}^i_{s1} & \mathbf{k}^i_{s2} \\ 0 & (\mathbf{k}^i_{s2})^{\mathrm{T}} & \mathbf{k}^i_{s3} \end{bmatrix}, \tag{14}$$

where

$$\mathbf{k}^i_u = \int_{S_{\mathrm{m}}} (\mathbf{B}^u)^{\mathrm{T}} \mathbf{A}^i \mathbf{B}^u\, \mathrm{d}S_{\mathrm{m}}, \tag{15}$$

$$\mathbf{k}^i_b = \int_{S_{\mathrm{m}}} (\mathbf{B}^\phi)^{\mathrm{T}} \boldsymbol{T}^{\mathrm{T}} \mathbf{D}^i \boldsymbol{T} \mathbf{B}^\phi\, \mathrm{d}S_{\mathrm{m}},$$

$$\mathbf{k}^i_{s1} = \int_{S_{\mathrm{m}}} (\mathbf{B}^{s1})^{\mathrm{T}} \mathbf{C}^i \mathbf{B}^{s1}\, \mathrm{d}S_{\mathrm{m}},$$

$$\mathbf{k}^i_{s2} = \int_{S_{\mathrm{m}}} (\mathbf{B}^{s1})^{\mathrm{T}} \mathbf{C}^i \mathbf{B}^{s2}\, \mathrm{d}S_{\mathrm{m}},$$

$$\mathbf{k}^i_{s3} = \int_{S_{\mathrm{m}}} (\mathbf{B}^{s2})^{\mathrm{T}} \mathbf{C}^i \mathbf{B}^{s2}\, \mathrm{d}S_{\mathrm{m}}.$$

To satisfy the continuity of in-plane displacements at the ply interfaces, we use Eq. (2) to define the matrix of constraints $\mathbf{Q}^i$ and the Lagrange multipliers $\boldsymbol{\lambda}^i = (\lambda^i_1, \lambda^i_2, \lambda^i_3)^{\mathrm{T}}$, which represent the nodal forces at the ply interfaces.

2.4. System of equations

After the standard assembly process the resulting system of equations can be written as

$$\mathbf{K}\mathbf{d} + \mathbf{Q}^{\mathrm{T}}\boldsymbol{\lambda} = \mathbf{f}, \qquad \mathbf{Q}\mathbf{d} = \mathbf{0}, \tag{16}$$

where the matrix of constraints $\mathbf{Q}$ may be split by vertical lines into blocks $\mathbf{Q}^i$ that comply with the block structure of $\mathbf{K}$ so that each block $\mathbf{Q}^i$ comprises the part of constraints that are related to the ith layer. To solve system (16), it is important to observe that the matrix $\mathbf{K}$ is block diagonal with symmetric positive definite blocks $\mathbf{K}^i$ corresponding to

layers, and that the matrix $\mathbf{Q}$ is sparse. Moreover, the matrices $\mathbf{K}^i$ are banded so that they may be effectively decomposed by the Cholesky or $\mathbf{LDL}^{\mathrm{T}}$ factorization.

Though the matrix of system (16) is sparse and has a regular sparsity pattern, it is obvious that its solution by a variant of the Gauss elimination is not efficient due to the fill-in [2]. For example on a computer with 128 MB RAM, the 6-layer composite plate discretized by mesh of 16×16 elements may be treated as a maximum. Moreover, since the matrix of the system is indefinite, it is difficult to find an efficient pre-conditioner for application of the standard iterative methods.

3. Solution of the system of equations

Similarity of system (16) to the system arising from application of the basic FETI algorithm rises a question whether we could apply a variant of the basic FETI method [4,8] to its solution. Let us recall that to solve Eq. (16) by a FETI like method, we should eliminate the primal variables $\mathbf{d}$ from Eq. (16) and then the resulting system is solved by the conjugate gradient method [12]. This approach may be more efficient than the application of a direct solver and does not require large number of iterations. Moreover, the matrix of the resulting system and the Schur complement with respect to $\boldsymbol{\lambda}$ can be kept in the form of products of several matrices [4,8]. In this section, we shall explain implementation of the proposed variant of the FETI like approach that results in an effective solution of Eq. (16).

3.1. FETI and decomposition into layers

We start by rewriting the system of equations (16) in more detail as

$$\forall i \in \{1,\ldots,N\} \quad \mathbf{K}^i\mathbf{d}^i = \mathbf{f}^i - (\mathbf{Q}^i)^{\mathrm{T}}\boldsymbol{\lambda}, \tag{17}$$

$$\sum_{i=1}^{N} \mathbf{Q}^i\mathbf{d}^i = \mathbf{0} \tag{18}$$

and the vector of unknown displacements $\mathbf{d}^i$ can be expressed from Eq. (17) in the form

$$\mathbf{d}^i = (\mathbf{K}^i)^{-1}(\mathbf{f}^i - (\mathbf{Q}^i)^{\mathrm{T}}\boldsymbol{\lambda}). \tag{19}$$

The unknown vectors $\mathbf{d}^i$ can be substituted in Eq. (18) to get

$$\sum_{i=1}^{N} \mathbf{Q}^i(\mathbf{K}^i)^{-1}(\mathbf{Q}^i)^{\mathrm{T}}\boldsymbol{\lambda} = \sum_{i=1}^{N} \mathbf{Q}^i(\mathbf{K}^i)^{-1}\mathbf{f}^i. \tag{20}$$

As mentioned above, Eq. (20) resembles the one arising from the application of the FETI method to the different problems. However, a closer inspection of the structure and the meaning of the Lagrange multipliers reveal the essential differences. In particular, our multipliers join the nodes in the adjacent layers, not only the boundary ones and the theoretical results related to the standard FETI method for plates [9,10] cannot be applied directly to our case.

The number of multipliers and the resulting order of Eq. (20) is much greater than that of the original FETI method. Moreover, the multipliers join displacements between the plies, therefore the structure of the matrix $\mathbf{Q}$ differs from the FETI method as well. As a result, we can hardly assume that the spectrum of the matrix $\mathbf{QK}^{-1}\mathbf{Q}^{\mathrm{T}}$ will be so favorably distributed as in the case of the FETI method [13]. In fact, our experiments with the solution of the system by the basic FETI algorithm appeared to be extremely inefficient even for the solution of modest problems [7]. The results were not much better even with the standard lumped pre-conditioner [14].

3.2. Orthonormalization of constraints

The unsuccessful experiments with the basic FETI method led us to an improvement to our knowledge not used so far in the context of the FETI method. First notice that Eq. (18) is equivalent to

$$\mathbf{RQd} = \mathbf{0} \tag{21}$$

with any regular matrix $\mathbf{R}$. In particular, taking for $\mathbf{R}$ the matrix that implements the Schmidt orthonormalization, we can achieve that the matrix $\mathbf{H} = \mathbf{RQ}$ has orthonormal rows and

$$\mathbf{Hd} = \mathbf{0} \tag{22}$$

is equivalent to Eq. (21). Moreover, the specific form of matrix $\mathbf{Q}$ allows effective implementation of the Schmidt orthonormalization, thus the sparsity pattern of $\mathbf{Q}$ is properly exploited. More details may be found in Section 3.3. As a result of the orthonormalization, after imposing the block structure of the matrix $\mathbf{Q}$ on the matrix $\mathbf{H}$, we get the system

$$\sum_{i=1}^{N} \mathbf{H}^i(\mathbf{K}^i)^{-1}(\mathbf{H}^i)^{\mathrm{T}}\boldsymbol{\lambda} = \sum_{i=1}^{N} \mathbf{H}^i(\mathbf{K}^i)^{-1}\mathbf{f}^i, \tag{23}$$

which looks similar with Eq. (20), except that the matrix $\mathbf{Q}$ was replaced by the matrix $\mathbf{H}$ with orthonormal rows. It may be observed that for the matrix $\mathbf{HK}^{-1}\mathbf{H}^{\mathrm{T}}$ it is possible to give tighter bounds on spectrum as compared to $\mathbf{QK}^{-1}\mathbf{Q}^{\mathrm{T}}$. From the equality

$$\frac{\boldsymbol{\lambda}^{\mathrm{T}}(\mathbf{HK}^{-1}\mathbf{H}^{\mathrm{T}})\boldsymbol{\lambda}}{\boldsymbol{\lambda}^{\mathrm{T}}\boldsymbol{\lambda}} = \frac{(\mathbf{H}^{\mathrm{T}}\boldsymbol{\lambda})^{\mathrm{T}}\mathbf{K}^{-1}(\mathbf{H}^{\mathrm{T}}\boldsymbol{\lambda})}{(\mathbf{H}^{\mathrm{T}}\boldsymbol{\lambda})^{\mathrm{T}}\mathbf{H}^{\mathrm{T}}\boldsymbol{\lambda}}, \tag{24}$$

which is valid for any non-zero vector $\boldsymbol{\lambda}$ follows that any Rayleigh quotient of the matrix $\mathbf{HK}^{-1}\mathbf{H}^{\mathrm{T}}$ is also the Rayleigh quotient of the matrix $\mathbf{K}^{-1}$. Thus the spectrum of $\mathbf{HK}^{-1}\mathbf{H}^{\mathrm{T}}$ is always within the bounds of the spectrum of $\mathbf{K}^{-1}$, while there is only little probability that similar inclusion is valid for the matrix $\mathbf{QK}^{-1}\mathbf{Q}^{\mathrm{T}}$. The spectral condition number of the matrix $\mathbf{HK}^{-1}\mathbf{H}^{\mathrm{T}}$ may be shown to depend on the angle between the range of the matrix $\mathbf{H}^{\mathrm{T}}$ and

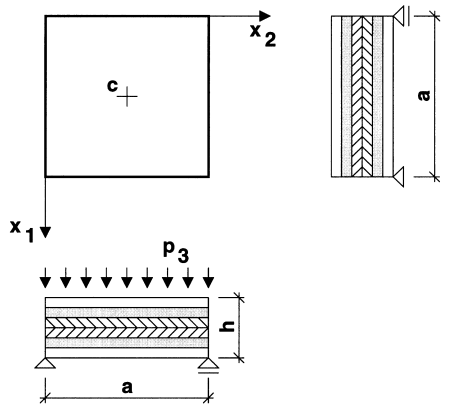

Fig. 3. Example of six layers simply supported plate.

the subspace spanned by the eigenvectors corresponding to the extreme eigenvalues of the matrix $\mathbf{K}$ [11]. We conclude that it is natural to expect that the spectral properties of the matrix $\mathbf{H}\mathbf{K}^{-1}\mathbf{H}^{\mathrm{T}}$ are more favorable for application of the conjugate gradient method to those of $\mathbf{Q}\mathbf{K}^{-1}\mathbf{Q}^{\mathrm{T}}$.

Our experiments confirmed that the orthonormalization of the constraints described above improved considerably the rate of convergence of the conjugate gradient method for the solution of the reduced system of equations. The rate of convergence was further improved by application of the lumped pre-conditioner $\mathbf{Y}^{-1} = \mathbf{H}\mathbf{K}\mathbf{H}^{\mathrm{T}}$. The results reported in Section 4 were achieved with the untransformed pre-conditioned conjugate gradient method [12] with the lumped pre-conditioner applied to the system $\mathbf{H}\mathbf{K}^{-1}\mathbf{H}^{\mathrm{T}}$.

It seems that a simple observation with the orthonormalization of constraints has not been used in the FETI method, though the multiplication of the matrix of constraints by a diagonal weighting factors was proposed at the very beginning of the FETI method [4]. The efficiency of our approach is also indicated by recent results by Klawonn and Widlund [15] who used a slightly different procedure to get an orthogonal projector between the matrix and a pre-conditioner. The very strong asymptotic estimates for the rate of convergence were proved as well. Let us mention that orthonormalization of constraints has been successfully used in paper on the solution of variational inequalities by the FETI [16].

3.3. Parallel implementation

As mentioned above, our method of discretization of layered plates is closely related to the FETI domain decomposition method. The plate is divided by horizontal planes so that the subdomains are formed by layers. Thus it is natural to assign all the information concerning one subdomain to one processor. Such choice enables us to implement the conjugate gradient method for the solution of system (23) in parallel, with the high degree of parallel scalability.

Orthonormalization of constraints has a crucial influence on the number of iterations. Therefore the important part of our algorithm is efficient implementation of the Schmidt orthonormalization. To this end, it is important to recall that the resulting matrix of constraints is created by blocks defined on subdomains. Moreover, each block has a special regular pattern and has only two non-zero entries per row. Thanks to regularity of the blocks, the orthonormalization process can be done efficiently on the sparse matrix storage as there are not more than $2N$ non-zero entries in the row after orthonormalization, where N is the number of subdomains. This is consequence of our option to define multipliers in the nodes. If the multipliers were defined on an element [2], the resulting orthonormal matrix would be a full lower triangular matrix.

3.4. Convergence

The FETI was proposed as a domain decomposition method for elliptic partial differential equation problems by Farhat and Roux [4] and the description of the convergence properties are summarized in Ref. [17]. The condition numbers are bounded by expression $C(1 + \log(H/\tilde{h}))^{\gamma}$, where H is the size of subdomain, $\tilde{h}$ denotes the characteristic size of an element and γ is equal to 2 or 3. These bounds are valid for linear conforming elements and the Dirichlet pre-conditioners applied to the second order problems. The polylogarithmical increase of the condition number was proved also for the fourth order problems and holds for a broad class of bending elements.

The plate problems are generally analyzed by iterative solvers with difficulties, because the corresponding condition numbers are usually very high. The stiffness of the composite material differs with respect to the fiber orientation and a large variation of the entries in the element stiffness matrix deteriorates the condition number further.

The proposed numerical model based on the refined layered theory and modified FETI algorithm is robust, as is demonstrated in the numerical experiments. The number of iterations grows very slowly and for the domain discretized by regular meshes with general material properties the growing of iterations is logarithmical. The increase in the number of iterations for a general domain discretized by unstructured mesh with general material properties is not so smooth as for a regular one, but the logarithmical curve can be obtained after smoothing.

4. Examples

To demonstrate the performance of the proposed model and solver we first consider a simple domain supported by simple boundary conditions. The geometry and loading are shown in Fig. 3, where $a = 1.500$ m, $h = 0.027$ m and uniform compression $p_3 = 50.0$ kPa.

Only one quarter of this plate with lay-up $[0, 60, 90]_s$ is computed due to the symmetry. The number of layers is six,

Table 1
Material properties in GPa

Material	E_L	E_T	G_L	G_T	$(\nu$
T-50 graphite	386.4	7.6	15.2	2.6	0.41
6061 Aluminum	72.5	72.5	27.3	27.3	0.33

so that the thicknesses of layers are $h^i = 4.5$ mm. Each ply is made of aligned T-50 graphite fibers bounded to the 6061 Aluminum matrix with volume fraction $c_f = 0.5$. The material properties are listed in Table 1. Overall properties are obtained by the Mori–Tanaka [18,19] averaging method.

The plate was discretized by several regular meshes which are characterized in Table 2 by the resulting number of degrees of freedom (Dof), the number of unknown Lagrange multipliers (Mult) and non-zero entries of the stiffness matrix (Nem) on one subdomain. In all computations, we used a stop criterion based on relative precision

$$\frac{\|\mathbf{r}\|^2}{\|\mathbf{b}\|^2} < \varepsilon = 10^{-10}, \tag{25}$$

where the error is measured in the Euclidean norm. The dependency of the total number of iterations on the total number of Dof + Mult is shown in Fig. 4, where $5 \times 5,\ldots,70 \times 70$ represent corresponding element mesh configurations. This curve resembles the logarithmical curve, which was obtained for FETI in Ref. [17].

The performance for the general domain is shown in Fig. 5. A mesh consisting of three node elements was generated using the T3D generator developed by Rypl [20]. The structure was clamped on the external perimeter and loaded by forces on the internal vertexes. There are six layers in this example and the thickness of one layer is $h^i = 5.0$ mm. Material properties are the same as in the previous example and are listed in Table 1. The deformation of the structure is shown in Fig. 6. Fig. 7 shows the dependency of the number of iterations on the total number of degrees of freedom, where Nel denotes number of elements used in discretization.

For the performance evaluation the *user* and *system* together with the *real* times are compared. The time of communication steps is incorporated in the *system* time while the computational work in the *user* time. From Figs. 8 and 9 it is clear that the communication on the massive parallel computer IBM SP2 is more efficient than on the cluster of PCs. The system time is even higher than the user time for small problems on the cluster. This result is in accordance with the rule for parallel processing which asserts that the RAM of the processors has to be used as much as possible and the number of communications has to be minimized.

Table 2
Several types of discretization

Mesh	Dof	Mult	Nem
5×5	750	375	3355
10×10	3000	1500	26,420
20×20	12,000	6000	206,725
30×30	27,000	13,500	690,930
40×40	48,000	24,000	1,629,035
50×50	75,000	37,500	3,171,040
60×60	108,000	54,000	5,466,945
70×70	147,000	73,500	8,666,750

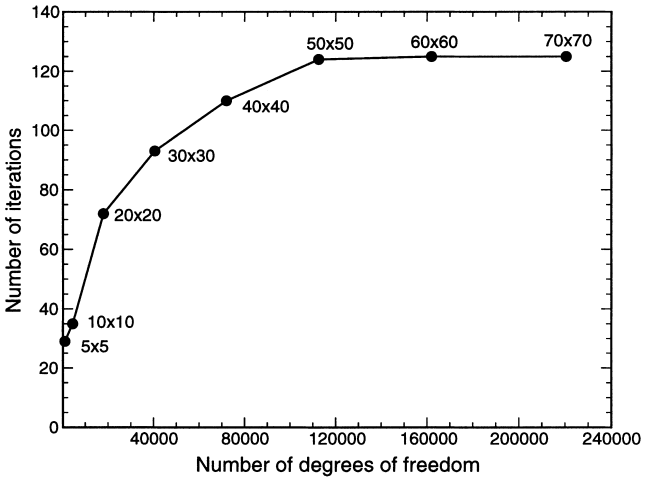

Fig. 4. Convergence behavior; example no. 1.

5. Conclusions

We have presented a model of composite laminated plates and its discretization. The process combines a natural layer-by-layer discretization approach with the parallel technique that solves the problem in a similar way.

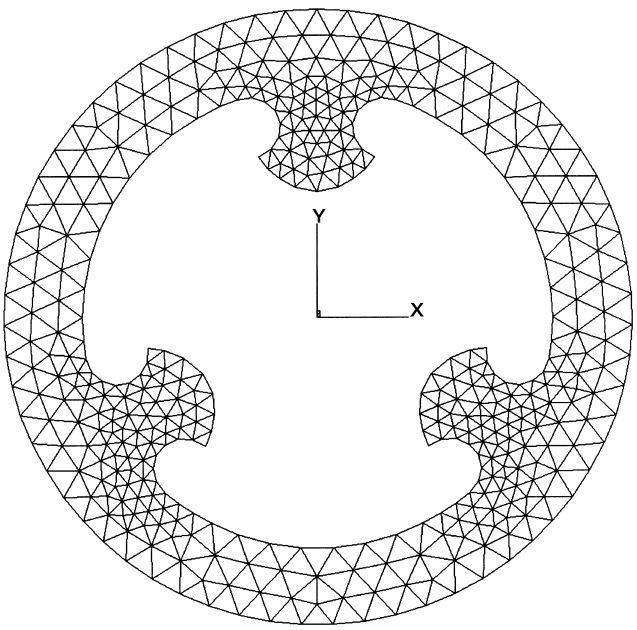

Fig. 5. General domain.

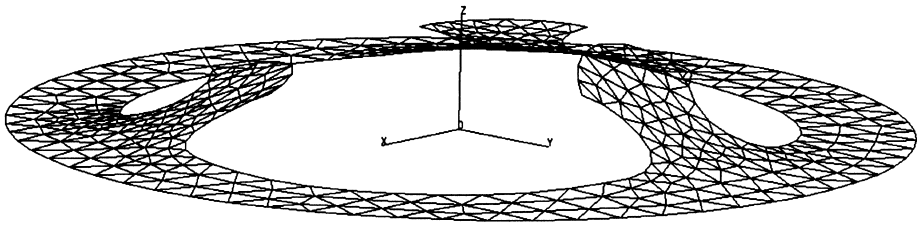

Fig. 6. Deformation of the plate.

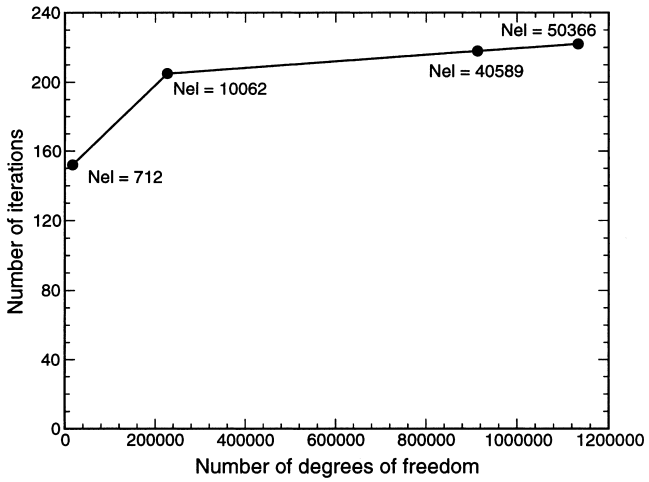

Fig. 7. Convergence behavior; example no. 2.

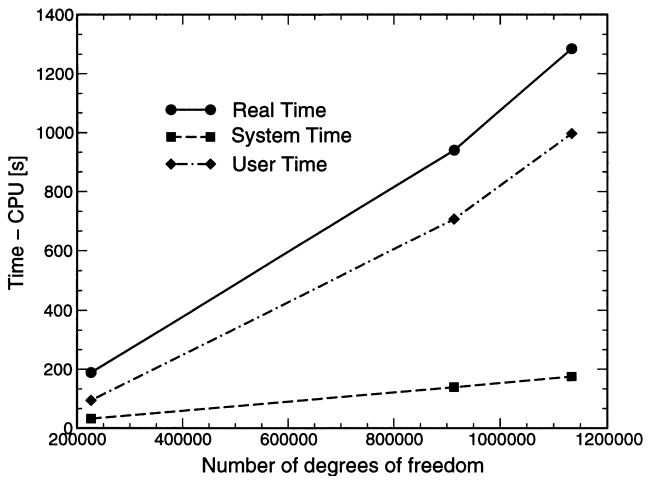

Fig. 8. Running times on IBM SP2.

New modification of the basic FETI method with the orthonormalization of constraints was used for the solution of the resulting system of equations. The results of the numerical experiments presented in this paper indicate that there are problems of practical interest that may be solved using this method. The work in progress extends this approach to enhance the decomposition of each layer, the more general boundary conditions and the pre-conditioning by the natural coarse grid. Such generalization of the approach has been developed and analyzed in Ref. [14].

The results obtained for both examples indicate a nice numerical scalability and efficiency of the proposed numerical model and solver to large areas of laminated composite materials and structures.

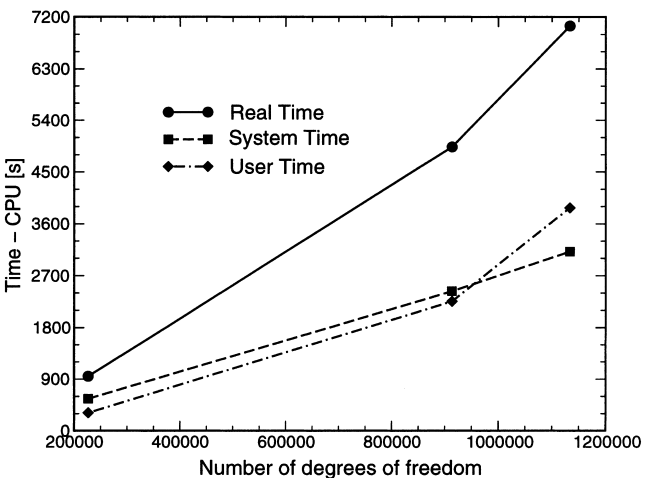

Fig. 9. Running times on DELL computers.

Acknowledgements

Financial support for this work was provided by the grant GAČR 103/01/0400 and the Ministry of Education of Czech Republic J04/98:210000003. Their financial assistance is gratefully acknowledged.

References

[1] Mau ST. Refined laminated plate theory. J Appl Mech 1973;606–7.
[2] Šejnoha M. Laminated 4-node plate element based on refined theory. Acta Polytech 1998;38(1):63–74.
[3] Hughes TJR. The finite element method, linear static and dynamic finite element analysis. New Jersey: Prentice-Hall, Inc., a division of Simon & Schuster; 1987.
[4] Farhat C, Roux FX. Implicit parallel processing in structural mechanics. Comput Mech Adv 1994;2:1–124.
[5] Papadrakakis M. Parallel solution methods in computational mechanics. Chichester: Wiley; 1997.
[6] Matouš K. Analysis and optimization of composite materials and structures. CTU Rep 2000;3(4).
[7] Kruis J, Matouš K. Applying FETI to composite laminated plates. In: Marek I, editor. Proceeding of the XIIIth Summer School Software and Algorithms of Numerical Mathematics, Nečtiny; 1999.
[8] Farhat C, Roux FX. The Dual Schur complement method with well

posed local Neumann problems. SIAM J Sci Stat Comput 1993;14: 752–9.
[9] Mandel J, Tezaur R, Farhat C. A scalable substructuring method by Lagrange multipliers for plate bending problems. SIAM J Numer Anal 1999;36(5):1370–91.
[10] Farhat C, Mandel J. The two-level FETI method for static and dynamic plate problems. I. An optimal iterative solver for biharmonic systems. Comput Meth Appl Mech Engng 1998; 155(1/2):129–51.
[11] Dostál Z. Conjugate gradient method with preconditioning by projector. Int J Comput Math 1988;23:315–24.
[12] Axelsson O. Iterative solution methods. Cambridge: Cambridge University Press; 1995.
[13] Roux FX. Spectral analysis of interface operator. In: Keyes DE, editor. Domain decomposition methods for partial differential equations. Philadelphia: SIAM; 1992.
[14] Farhat C, Mandel J, Roux FX. Optimal convergence of the FETI domain decomposition method. Comput Meth Appl Mech Engng 1993;115:365–85.
[15] Klawonn A, Widlund O. A domain decomposition method with Lagrange multipliers for linear elasticity. Report number T.R. 780, Department of Computer Science, Courant Institute; 1999.
[16] Dostál Z, Neto FAMG, Santos SA. Solution of contact problems by FETI domain decomposition with natural coarse space projections. Comput Meth Appl Mech Engng 2000;190(13/14):1611–27.
[17] Tezaur R. Analysis of Lagrange multiplier based domain decomposition. PhD Thesis. University of Colorado at Denver; 1998.
[18] Benveniste Y. A new approach to the application of Mori–Tanaka's theory in composite materials. Mech Mater 1987;6:147–57.
[19] Dvorak GJ, Šejnoha M. Initial failure maps for ceramic and metal matrix composite laminates. Modelling Simul Mater Sci Engng 1996; 4:553–80.
[20] Rypl D. Sequential and parallel generation of unstructured 3D meshes. CTU Rep 1998;2(3).